Image-domain interferometry and wave-equation extended images

Ivan Vasconcelos
(ION Geophysical, GXT Imaging Solutions)

Paul Sava
(Center for Wave Phenomena, Colorado School of Mines)

Huub Douma
(ION Geophysical, GXT Imaging Solutions)

(January 19th, 2009)

Summary

Using general two- and one-way representations for scattered wavefields, we fully describe two- and one-way extended images obtained in wave-equation imaging. This formulation explicitly connects the wavefield correlations done in seismic imaging with the theory and practice of wavefield interferometry. We show that extended images actually behave as local scattered fields in the image domain. The wavefield behavior of two- and one-way extended images is illustrated using analytical and numerical examples. The general description of extended images presented here may prove to be useful in further developing imaging and inversion methods.

Introduction

Most imaging methods based on wavefield extrapolation rely on the cross-correlation of source and receiver wavefields to invoke the zero-lag imaging condition (e.g., Claerbout, 1985). An extension of the zero-lag imaging concept is to perform wavefield correlations with nonzero lags in space coordinates (e.g., Sava and Fomel, 2003), which allows for the analysis of image-domain gathers that has now become a relatively common practice in exploration seismic imaging. Recently, fully extended images (e.g., Sava and Vasconcelos, 2009) have been proposed, now accounting for wavefield correlations that have nonzero lag both in space and time coordinates.

In the field of seismic interferometry (e.g., Curtis et al., 2006; Vasconcelos and Snieder, 2008), cross-correlations are used to extract the response between receivers as if one of them acts as a source. Through the use of scattering representations (e.g., Vasconcelos and Snieder, 2008; Wapenaar et al., 2008), interferometry can be tailored to extract only the scattered waves propagating between points in the medium. Vasconcelos (2008) used a two-way scattering representation to demonstrate that the imaging condition in wave-equation migration (e.g., Claerbout, 1985) can also be thought of as interferometry: the image is the zero-time scattered-wave response generated by zero-offset pseudo-experiments in the image domain. In this paper, we expand on the concept of image-domain interferometry and use general scattering reciprocity to provide exact descriptions of the two- and one-way extended images in wave-equation migration.

Scattering representations for two- and one-way acoustic waves

Two-way scattered fields.

Let the scattered-field impulse response G_S be defined by the difference of a total perturbed field G and a reference field G_0, i.e., $G_S = G - G_0$. The frequency-domain scattered-wave response $G_S(\mathbf{r}_B, \mathbf{r}_A)$, describing scattered waves propagating between any to points $\mathbf{r}_B$ and $\mathbf{r}_A$, is given by (Vasconcelos, 2007; Vasconcelos and Snieder, 2008)

$$
\begin{aligned}
G_S(\mathbf{r}_B, \mathbf{r}_A, \omega) &= \oint_{\mathbf{r} \in \partial \mathbb{V}} \frac{1}{i\omega\rho} \left[G_S(\mathbf{r}, \mathbf{r}_A, \omega) \nabla G_0^*(\mathbf{r}, \mathbf{r}_B, \omega) + G_0^*(\mathbf{r}, \mathbf{r}_B, \omega) \nabla G_S(\mathbf{r}, \mathbf{r}_A, \omega) \right] \cdot \mathbf{n} \, d^2\mathbf{r} \\
&+ \int_{\mathbf{r} \in \mathbb{V}} \frac{1}{i\omega\rho} G(\mathbf{r}, \mathbf{r}_A, \omega) \mathcal{V}(\mathbf{r}) G_0^*(\mathbf{r}, \mathbf{r}_B, \omega) \, d^3\mathbf{r} \, ;
\end{aligned}
\tag{1}
$$

where $\partial \mathbb{V}$ is a smooth surface (with outward-pointing normals $\mathbf{n}$) enclosing some volume $\mathbb{V}$. Here, ω is the harmonic frequency and ρ denotes spatially-varying density. The *scattering potential* $\mathcal{V} = \omega^2(c^{-2} - c_0^{-2})$ describes the scattering properties of the medium in terms of the wavespeed contrast between the reference (c_0) and perturbed (c) media.

One-way scattered fields.

Now we assume that a given pressure wavefield p (not necessarily impulsive) can be decomposed in an up-going component p^- and a down-going component p^+ (e.g., Wapenaar et al., 2008). These general up- and down-going fields can be related with the reflectivity operator R_0^+, which describes the up-going scattering response due a single downgoing reference field. The relationship between all these fields is given, in the frequency domain, by the following convolution-type theorem:

$$
p^-(\mathbf{r}_A, \mathbf{r}_S) = \int_{\partial \mathbb{V}_1} R_0^+(\mathbf{r}_A, \mathbf{r}) \, p^+(\mathbf{r}, \mathbf{r}_S) \, d^2\mathbf{r} \, ;
\tag{2}
$$

where $\partial \mathbb{V}_1$ is a horizontal plane of integration. Note that the equation describes the up-going pressure field p^- as a multidimensional convolution between p^+ and the desired reflectivity response R_0^+.

Extended imaging conditions for two- and one-way migration

Two-way imaging conditions.

An image can be defined as the zero-offset scattered-wave response evaluated at every point $\mathbf{r}_I$ in the image space and at time equal zero (Claerbout, 1985). To impose this image criterion, we can simply use the exact representation in equation 1 in the identity $\mathcal{I}(\mathbf{r}_I) = G_S(\mathbf{r}_I, \mathbf{r}_I, t = 0) = \int G_S(\mathbf{r}_I, \mathbf{r}_I, \omega) \, d\omega$. While interferometry relies on observed fields G_0 and G_S (e.g., Vasconcelos, 2008), in wave-equation imaging these fields result from extrapolating (i.e., re-datuming) the fields recorded at the acquisition surface to the image point $\mathbf{r}_I$ (e.g., Claerbout, 1985; Sava and Vasconcelos, 2009). In imaging, $G_0(\mathbf{r}, \mathbf{r}_I, \omega)$ are depth-extrapolated source wavefields, while $G_S(\mathbf{r}, \mathbf{r}_I, \omega)$ are the image-domain scattered fields extrapolated from the recorded data. In conventional common-shot wave-equation migration (e.g., Claerbout, 1985; Sava and Vasconcelos, 2009), the cross-correlation of source and receiver fields followed by summation over shots at the surface corresponds to the evaluation of the surface integral in equation 1.

The volume term in equation 1 is not explicitly evaluated in most conventional wave-equation migration methods (Vasconcelos, 2008). Using equation 1 to define an image in two-way wave-equation migration according to the imaging condition above (Vasconcelos, 2008), we define an extended image (e.g., Sava and Vasconcelos, 2009) as

$$
\begin{aligned}
\mathcal{I}'(\mathbf{r}_I, \delta\mathbf{r}', \tau) \;=\;& G_S(\mathbf{r}_I - \delta\mathbf{r}', \mathbf{r}_I + \delta\mathbf{r}', t = \tau) \\
=\;& \int e^{i\omega\tau}\, d\omega \oint_{\mathbf{r} \in \partial\mathbb{V}} \frac{2}{\rho c}\, G_S(\mathbf{r}, \mathbf{r}_I + \delta\mathbf{r}', \omega)\, G_0^*(\mathbf{r}, \mathbf{r}_I - \delta\mathbf{r}', \omega)\, d^2\mathbf{r} \\
+\;& \int e^{i\omega\tau}\, d\omega \int_{\mathbf{r} \in \mathbb{V}} \frac{1}{i\omega\rho}\, G(\mathbf{r}, \mathbf{r}_I + \delta\mathbf{r}', \omega)\mathcal{V}(\mathbf{r})G_0^*(\mathbf{r}, \mathbf{r}_I - \delta\mathbf{r}', \omega)\, d^3\mathbf{r} \; ; \quad (3)
\end{aligned}
$$

where now the image is not only a function of $\mathbf{r}_I$, but also of the space-lag vector $\delta\mathbf{r}'$ and of the time-lag parameter τ. These are *the same* space- and time-lags discussed by Sava and Vasconcelos (2009). In deriving equation 3, we used a far-field radiation condition (e.g., Vasconcelos and Snieder, 2008) to manipulate the surface integral.

One-way imaging conditions.

The one-way convolution theorem in equation 2 can also be expressed in matrix-operator form, i.e., $\mathbf{P}^- = \mathbf{R}_0^+ \mathbf{P}^-$. It then follows that the reflectivity operator admits a Tykhonov regularized least-squares solution of the form: $\bar{\mathbf{R}}_0^+ = \mathbf{P}^-(\mathbf{P}^+)^\dagger \left[\mathbf{P}^+(\mathbf{P}^+)^\dagger + \epsilon^2\mathbf{\Delta}\right]^{-1}$; where $\dagger$ stands for the conjugate-transpose, $\mathbf{\Delta}$ is a regularization operator and ϵ is a weighting factor. By ignoring the inverse matrix, the reflectivity can be approximated as $\tilde{\mathbf{R}}_0^+ \approx \mathbf{P}^-(\mathbf{P}^+)^\dagger$. Note that this approximation relies solely in cross-correlations of up- with down-going fields. From the least-squares inverse response $\bar{\mathbf{R}}_0^+$ approximate response $\tilde{\mathbf{R}}_0^+$, we can define one-way extended images in a manner analogous to the two-way definition in equation 3. For example, a general one-way extended image based on wavefield correlations can be expressed as

$$
\begin{aligned}
I(\mathbf{r}_I, \mathbf{r}, \tau) \;=\;& \tilde{R}_0^+(\mathbf{r}_I, \mathbf{r}, t = \tau) \\
=\;& \int e^{i\omega\tau}\, d\omega \int_{\partial\mathbb{V}_S} p^-(\mathbf{r}_I, \mathbf{r}_S)\, \{p^+(\mathbf{r}_S, \mathbf{r})\}^*\, d^2\mathbf{r}_S . \quad (4)
\end{aligned}
$$

A one-way extended image analogous to that in equation 3 is obtained from equation 4 via $I'(\mathbf{r}_I, \delta\mathbf{r}', \tau) = \tilde{R}_0^+(\mathbf{r}_I - \delta\mathbf{r}', \mathbf{r}_I + \delta\mathbf{r}', t = \tau)$. Below we discuss how other types of extended images arise from the operator R_0^+.

Interpreting extended images

Two-way extended images.

According to equation 3, it is immediately explicit that the two-way extended images are, in fact, scattered wavefields with sources (at $\mathbf{r}_I - \delta\mathbf{r}'$) and receivers (at $\mathbf{r}_I + \delta\mathbf{r}'$) in the image-domain, and τ running as the time variable. Equation 3 defines a common-image-point extended images, i.e., both source and receiver points in the image-wavefield $G_S(\mathbf{r}_I - \delta\mathbf{r}', \mathbf{r}_I + \delta\mathbf{r}', \tau)$ vary for a fixed $\mathbf{r}_I$. We analyze this type of extended images because they are an extension of the more traditional common-image gathers used in wave-equation migration (e.g., Sava and Fomel, 2003; Sava and Vasconcelos, 2009). It is possible to conceive other types of extended images; for example, a common-source extended image, which would be given by $\mathcal{I}(\mathbf{r}_I, \delta\mathbf{r}, \tau) = G_S(\mathbf{r}_I, \mathbf{r}_I + \delta\mathbf{r}, \tau)$. In Figures 1a and 1b we show an example of the asymptotic phase behavior of the extended image in equation 3. In Figure 1a, when the image point is at the scatterer (i.e., $\mathbf{r}_I = \mathbf{x}_S$), the non-zero value of the extended image at the origin yields the traditional image. Away from the origin, Figure 1a depicts the traveltimes of transmitted scattered waves excited at $\mathbf{r}_I - \delta\mathbf{r}'$ and recorded at $\mathbf{r}_I + \delta\mathbf{r}'$. When $\mathbf{r}_I = \mathbf{x}_S$ (Figure 1b), the extended image vanishes at the origin, but it instead shows the traveltimes of waves scattered at $\mathbf{x}_S$.

One-way extended images.

Analogous to their two-way counterparts, one-way extended images also behave as wavefields, described by the reflectivity operator R_0^+ (equation 2). In Figure 2a, we show R_0^+ at a given image depth in explicit matrix form. The image points which act as pseudo-sources ($\mathbf{r}_I$) belong to the column space of the matrix, whereas the image points acting as receivers ($\mathbf{r}$) are the rows of the matrix. The conventional zero-lag image lies in the principal diagonal of R_0^+ (highlighted with black dots). Extended images are obtained by including off-diagonal elements of R_0^+. Note that, for depth-domain one way extrapolation, the off-diagonal elements in Figure 2a correspond to horizontal lags only. The matrix columns (in blue) yield image gathers of the common-source type, while the data in the rows (in green) result in common-receiver image-gathers. The more traditional common-image-point gathers, $I'(\mathbf{r}_I, \delta\mathbf{r}', \tau = 0)$ are given by the diagonal elements highlighted in red.

Ideally, the one-way extended images should be estimated through a multidimensional deconvolution process at every depth, as described above. Here, however, we focus on the behavior of the approximate correlation-based extended images, described by equation 4. Figures 1c and 1d show the predicted phase of one-way extended images in the single scatterer case. Since R_0^+, and consequently the extended image, satisfy pseudodifferential wave equations (e.g., Wapenaar and Grimbergen, 1996) its response is nonzero only in a limited range of propagation directions. This is why the one-way responses in Figures 1c and 1d are essentially limited-aperture versions of the two-way images in Figures 1a and 1b.

To further elucidate the behavior of the extended image $I'(\mathbf{r}_I, \delta\mathbf{r}', \tau)$, we illustrate the stationary contributions to the integrand in Figures 2b and 2c. For point diffractors (Figure 2), there are many stationary sources (e.g., both $\mathbf{r}'_S$ and $\mathbf{r}''_S$). For any pair $(\mathbf{r}_I - \delta\mathbf{r}', \mathbf{r}_I + \delta\mathbf{r}')$ lying on a stationary path (solid lines in Figure 2b), there is a contribution to the extended image at $\tau = 0$ because the up-going field at $\mathbf{r}_I - \delta\mathbf{r}'$ has the same traveltime as the down-going wave at $\mathbf{r}_I + \delta\mathbf{r}'$. Thus, for varying $\delta\mathbf{r}'$, every stationary source yields a non-zero contribution along a straight line in the $[\delta\mathbf{r}'_1, \delta\mathbf{r}'_2]$-plane that coincides with the stationary path. In the single-scatterer case (Figure 2b), the superposition of many such straight lines associated to all available stationary points effectively results in a band-limited point in an extended image at $\mathbf{r}_I = \mathbf{x}_S$ (see also Figure 1c). This scenario changes if the waves are scattered by a horizontal interface, as in Figure 2c. In that case, the only stationary source contribution is at $\mathbf{r}'_S$ which yields a stationary path along a straight vertical line (Figure 2c). So, unlike the point-scatterer case, the extended image corresponding to Figure 2c will depict a straight line in the $[\delta\mathbf{r}'_1, \delta\mathbf{r}'_2]$-plane that is always perpendicular to the interface: a vertical line in this case.

In Figure 3, we show a numerical example of the one-way extended images. The model contains point scatterers as well as horizontal and dipping interfaces (Figure 3a). We show the extended images (Figures 3b through 3d) at three different locations in the conventional image (red points in Figure 3a). At the point diffractor (Figure 3a) and using the correct wavespeed model, the one-way extended image response is a band-limited point at the origin. This agrees with our analysis of the behavior one-way extended images based in Figures 2b and 1c. Also, as explained using the cartoon in Figure 2c, the one-way extended images at the interfaces (Figures 3c and 3d) focus around $\tau = 0$ and along straight lines that are perpendicular to the local interface dip.

Conclusion

Based on scattering representations, wave-equation extended images are effectively described as local scattered wavefields in the image space. By describing extended images as local wavefields, we offer a a generalized formulation to perform image-domain analyses that can bring many potential advantages. First, in principle, our formulation allows for inclusion of the effects of multiple scattering and transmission, e.g., for potential migration of free-surface or internal multiples. Second, extended images may help in formally describing and treating migration/imaging artifacts such as, for instance, the commonly observed artifacts caused by sharp model contrasts in reverse-time migration. Finally, extended images as described here possibly allow for further development of image-domain inversion for reflectivity and/or wavespeed models. Indeed, Sava and Vasconcelos (2009) demonstrate that the extended images described here may provide additional sensitivity to the background migration wavespeed model and can therefore be exploited for the purposes of wave-equation tomography.

References

[1] J.F. Claerbout. Imaging the Earth's Interior. *Blackwell Publishing*, 1985.

[2] Curtis, A., Gerstoft, P., Sato, H., Snieder, R. and K. Wapenaar, Seismic interferometry – turning noise into signal: The Leading Edge, 25, 1082–1092, 2006.

[3] P. Sava and S. Fomel. Angle-domain common-image gathers by wavefield continuation methods. *Geophysics*, 68:1065-1074, 2003.

[4] P. Sava and I.Vasconcelos. Extended common-image-point gathers for wave-equation migration. *EAGE Exp. Abs*, 2009.

[5] I. Vasconcelos and R. Snieder. Interferometry by deconvolution, Part 1: Theory for acoustic waves and numerical examples. *Geophysics*, 73, S115–S128, 2008., 2008.

[6] I. Vasconcelos. Generalized representations of perturbed fields - Applications in seismic interferometry and migration. *SEG Exp. Abs.*, 2008.

[7] K. Wapenaar, E. Slob and R. Snieder. Seismic and electromagnetic controlled-source interferometry in dissipative media *Geophysical Prospecting*, 56, 419–434, 2008.
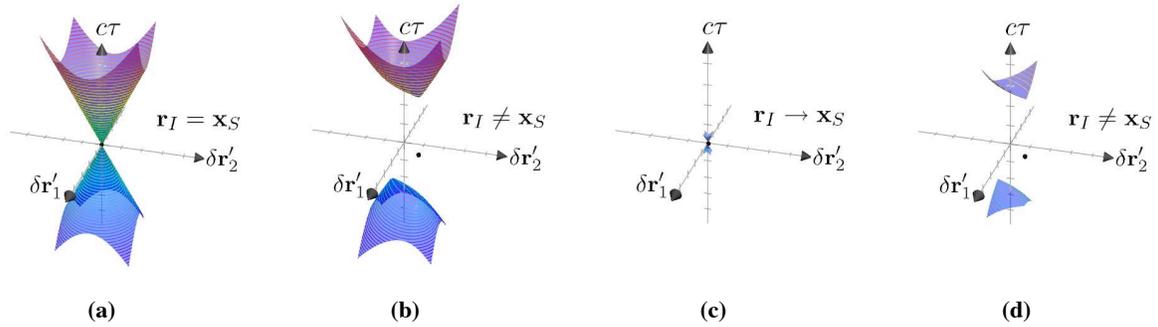
(a)   (b)   (c)   (d)

Figure 1: Asymptotic phase behavior of common-image-point extended images (at $\mathbf{r}_I$) for the case of a single point scatterer at $\mathbf{x}_S$, embedded in a 2-D homogeneous space. Panels (a) and (b) represent the extended images of in two-way imaging (equation 3), while (c) and (b) are the their one-way counterparts. These responses correspond to a medium with constant background wavespeed c. Note that the responses are depicted for normalized traveltimes $c\tau$. In all plots, the black dot illustrates the position of the scatterer (i.e. $\mathbf{x}_S$) with respect to the image point (i.e., $\mathbf{r}_I$ is always at the origin).
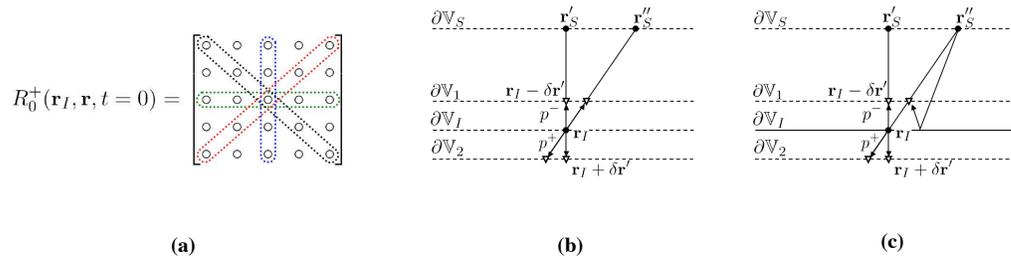

(a)   (b)   (c)

Figure 2: Behavior of one-way extended images. Panel (a) shows the structure of the zero-lag reflectivity operator R_0^+ in matrix form, at a given image level (e.g., for a fixed depth and with variable horizontal coordinates). Panels (b) and (c) relate to the behavior of one-way common-image-point extended images for the cases where scattering comes from a single scatterer, in (b), and from a plane horizontal interface, in (c). In both (b) and (c), the black dot denotes the image point $\mathbf{r}_I$, and triangles represent image-lag points $\mathbf{r}_I \pm \delta\mathbf{r}'$. The points $\mathbf{r}'_S$ and $\mathbf{r}''_S$ are two arbitrary source points from the integrand of equation 4.
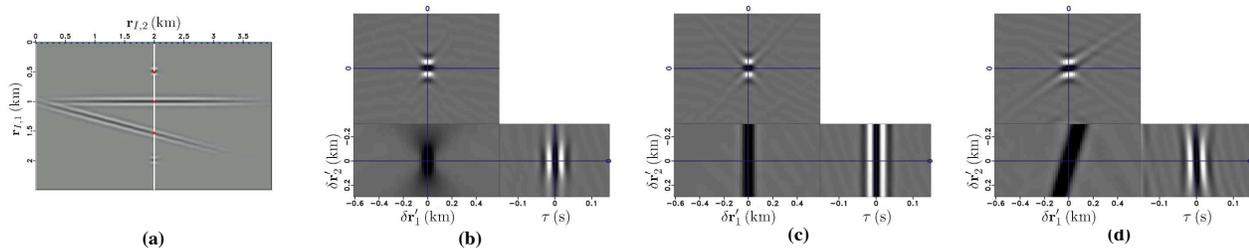

(a)   (b)   (c)   (d)

Figure 3: Numerical example of one-way extended images. Panel (a) is the conventional seismic image, where the red dots indicate the locations where extended images are evaluated. The corresponding extended images are shown in (b) at the point scatterer, in (c) at the horizontal reflector, and in (d) for the dipping reflector.